East European Journal of Physics. 2. 260-274 (2026)
DOI:10.26565/2312-4334-2026-2-28 ISSN 2312-4334

# INVESTIGATION OF STRUCTURAL, OPTOELECTRONIC AND PHOTOVOLTAIC PERFORMANCE OF $Cu_2SnS_3$COMPOUND: COMBINED DFT AND SCAPS-1D SIMULATIONS

**Boualem Kada[1], Karima Benyahia[1], Nabil Beloufa[2,3], Hamza Rekab-Djabri[2,4], D. Belfennache[5], Abdelkader Bouhenna[1], Samir Bekheira[2], A. Alami[6], Hamad M. Adress Hasan[7], Hamdy A. Khatab Ali[8]**

[1]*Materials Science and Applications Laboratory (LSMA), Faculty of Sciences and Technology, University of Ain-Temouchent, Algeria*
[2]*Laboratory of Micro and Nanophysics (LaMiN), National Polytechnic School of Oran, ENPO-MA, BP 1523, El M'Naouer, 31000, Oran, Algeria*
[3]*Hydrometeorological Institute for Training and Research IHFR, Ibnou Rochd.Bp 7019, Oran, Algeria*
[4]*Faculty of Nature and Life Sciences and Earth Sciences, AkliMohand-Oulhadj University, 10000, Bouira, Algeria*
[5]*Research Center in Industrial Technologies (CRTI) P.O. Box 64, Cheraga 16014 Algiers, Algeria*
[6]*Laboratory of Process Engineering, Materials and Environment, Faculty of Technology, University of DjillaliLiabes, P.O. Box 89, Sidi Bel Abbes 22000, Algeria;*
[7]*Chemistry Department, Faculty of Science, Omar Al-Mukhtar University, Libya*
[8]*Chemistry Department Faculty of Education (Al-Marj), Benghazi University, Libya*
**Correspondence Author e-mail: belfennachedjamel@gmail.com*
Received February 12, 2026; revised March 3, 2026; accepted May 6, 2026

Evaluating the structural, optoelectronic, and photovoltaic performance of the $Cu_2SnS_3$ compound is essential for the development of materials for solar energy. This ternary chalcogenide semiconductor stands out for its strong potential in photovoltaic applications, thanks to its broad light-absorbing range and chemical stability. In this paper, we have examined the structural and optoelectronic properties of copper-based ternary semiconductors, specifically those in the $Cu_2SnS_3$ compound, and their effectiveness in photovoltaic applications. Since there is significant variation in previous studies on the band gap values (0.65-1.35 eV), an attempt was made to find an appropriate approximation for studying this type of compound. The structural properties were investigated using both the Perdew-Burke-Ernzerhof (PBE) form of the generalized gradient approximation (GGA) and the local density approximation (LDA), allowing a comparative assessment of the effects of different exchange-correlation functionals on the material's structure. Given the important influence that Cu delectrons play in determining their electronic properties, as shown by the results obtained when using different exchange correlation energy functionals. The combined function of the Becke-Johnson potential, modified by Tran and Blaha, and the Hubbard potential (TB-mBJ+U) was employed to systematically optimize the calculated anion displacement. The calculations yielded the band gap values. The semiconductor quasiparticle is 0.7 eV in the monoclinic structure (m-CTS; SG: Cc), and that of the orthorhombic structure (gold-CTS; SG: Imm2) is 0.73 eV, which is largely consistent with experimental values. The study of optical properties, including the dielectric function, also revealed the reflectance, absorption coefficient, and refractive index of the $Cu_2SnS_3$ compound in its two phases. The latter is considered a promising candidate in optoelectronic applications. To verify this, we used the SCAPS program, and the results were good. When this compound is used as an absorbent layer in a photovoltaic cell, the current density (Jsc) increases, peaking at a thickness of 800 nm.
**Keywords:** *$Cu_2SnS_3$; FP-LAPW; LDA; TB-mBJ+U; Photovoltaic cells*
**PACS:** 73.50.-h, 73.50.Pz

## 1. INTRODUCTION

Semiconductors are attracting considerable interest due to their strong potential in photovoltaic applications, particularly for thin-film solar cells [1-3]. Among them, the chalcogenide family, especially copper chalcogenides and copper tin sulfide (CTS), is attracting increasing attention for their use in this type of device [4,5]. The preparation of these materials as colloidal inks can enable low-cost manufacturing via solution-based printing and coating processes [6, 7].

Due to the scarcity and rising prices of indium and gallium, there is interest in alternative chalcogenide semiconductors $Cu_2ZnSnSe_4$ (CZTSe) and $Cu_2ZnSnS_4$ (CZTS) [8,9]. The later solar panels have a relatively optimal efficiency of about 14% [10,11]. In practice, one could reduce the synthesis cost by incorporating tin and zinc at indium and gallium sites, respectively, in the CZTSe quaternary system. These later systems have very attractive applications as near-infrared devices [12], efficient Li-ion batteries [13,14], thermoelectric materials [15], and acousto-optic instrumentation. The CTSe compound is regarded as a promising material for solar panels, with a direct optical gap measured at 1.1-1.5 eV [16]. Several simple ternary systems exist, such as $Cu_2SnSe_3$, an example of a current low-cost solar cell. [17,18]. $Cu_2SnSe_3$ (CTSe) is a p-type semiconductor with an absorption coefficient greater than $10^4$ $cm^{-1}$ and a direct band gap between 0.8 and 1.1 eV. [19,20]. Compared to other solar cells, those based on CZTS ($Cu_2ZnSnS_4$) have achieved a maximum photovoltaic conversion efficiency of 12.6%. [21]. The CTS ($Cu_2SnS_3$) is a semiconductor interlayer compound that can be doped with zinc for the synthesis of CZTS ($Cu_2ZnSnS_4$). [22, 23]. CTS nanocrystals

***Cite as***: B. Kada, K. Benyahia, N. Beloufa, H. Rekab-Djabri, D. Belfennache, A. Bouhenna, S. Bekheira, A. Alami, H.M.A. Hasan, A.K.A. Hamdy, East Eur. J. Phys. 2, 260 (2026), https://doi.org/10.26565/2312-4334-2026-2-28

(NC) can themselves serve as absorbers for thin-film photovoltaic systems. [24] Therefore, the CTS system is composed of non-toxic, naturally abundant elements and is economically viable [25, 26]. Therefore, based on the latter considerations, this material is particularly relevant, both for its elaboration process and its attractive applications, such as solar panel technologies and precise optoelectronic devices. [27]. Actually, more research is focused on studying different absorber materials that exhibit excellent environmental performance and high-efficiency conversion panels [28,29]. Furthermore, the $Cu_2SnS_3$ (CTS) technology is a viable option, as it is composed of abundant, non-toxic elements. [30]. In the Cu-Sn-Se system, most research has been conducted on the ternary semiconductor $Cu_2SnSe_3$ [31]. The $Cu_2SnSe_3$ compound formed has a congruent melting point of 963 K [32] or 968 K [33].

$Cu_2SnS_3$ (CTS) remains one of the most promising ternary photo absorbing compounds [34, 35]. Because of its wide band gap and high optical absorption coefficient in the visible spectrum, it is a very attractive material for thin-film PV applications [36, 37]. The first PV device using the CTS compound as an absorber material was developed by T. A. Kuku and O. A. Fakolujo [38], with an efficiency of 0.11%. Since then, research on this material has almost stagnated, until a cell with an efficiency of 2.84% was reported by Koike et al. [39]. Studies conducted by Umehara et al. [40] have shown that it is possible to improve the efficiency of the CTS cell to 6.0% by doping it with germanium (Ge) using a $Cu_2Sn_{0.83}Ge_{0.17}S_3$ composition. CTS is a ternary semiconductor belonging to the I-IV-VI group [34]. It is a polymorphic material that crystallizes in various systems, namely cubic (F4-3m) with a=b=c=5.696Å [41], tetragonal I4-2d with a=b=5.689Å and c=11.370Å [42], monoclinic C1c1 with a=6.967Å, b=12.049Å, and c=6.945Å [31], and monoclinic superstructure C1c1 with a=6.961Å, b=12.043Å, and c=26.481Å [32].A hexagonal structure of CTS was reported by Wu et al. [43]. However, to date, no other study has reproduced this structure. Some rare research has been conducted on the synthesis of CTS with a triclinic phase. [44,45], and no detailed crystallographic description of this structure has been provided. Thus, the $Cu_2SnS_3$ compound exists in cubic, tetragonal, and monoclinic structures [34]. Furthermore, with the identification of copper-rich phases such as $Cu_3SnS_4$, $Cu_4SnS_4$, and $Cu_2S$, we obtain an increase in the conductivity of these materials. [46]. Robles et al. [47] demonstrate that the resistivity of CTS has been increased from $2.10^{-3}\Omega$.cm to $5.10^{-3}\Omega$.cm. Bodeux et al. [48] indicated that the variation in component content had an influence on the increase in CTS conductivity. They noted an increase from 0.1 S $cm^{-1}$ to 0.8 S $cm^{-1}$ for a Cu/Sn ratio that increased from 1.9 to 2.2. Thus, it is clear that the presence of secondary phases modifies the optical and electrical properties of the CTS compound and consequently affects the conversion efficiency of PV solar cells.

The thermodynamic study of CTS formation reveals that tetragonal and monoclinic structures form at relatively low temperatures (<750°C), whereas the cubic structure forms at higher temperatures (>750°C) [35]. Furthermore, cubic-structured CTS can also be produced experimentally at low temperatures using chemical synthesis methods by optimizing the experimental conditions [49]. Theoretically, calculations of the electronic density of states have all shown that CTS offers a direct optical aperture with theoretical values ranging from 0.84 eV to 0.88 eV [50, 51], while experimentally, the different optical gap values reported in the literature are in an extremely large range, from 0.83 to 1.77 eV [38,46,52], which are desirable values for PV applications. This compound also exhibits a strong optical absorption coefficient, with values reaching up to $10^5 cm^{-1}$[36, 52].

The originality of this study lies in the evaluation of the structural and optoelectronic properties of the $Cu_2SnS_3$ compound in both monoclinic (Cc) and orthorhombic (Imm2) structures using DFT and four approaches: LDA, GGA, GGA + U, and (TB-mBJ+U). Solar cell modeling based on CTS was performed using the 1-dimensional solar cell capacitance software (SCAPS-1D) to achieve optimal electrical conversion efficiency. The models studied take into account the influence of the thickness of the absorber coating on the behavior of the back contact, the effect of different parameters such as the thickness and concentration of doping of the various layers, as well as the design of a new $Cu_2SnS_3$ (CTS) based solar cell with a promising efficiency.

## 2. COMPUTATIONAL DETAILS

### 2.1 First-principle calculation of $Cu_2SnS_3$

Ab initio calculations were performed using the Full-Potential Linearized Augmented Plane Wave (FP-LAPW) method [53], as implemented in the Wien2k code [54], within the density functional theory (DFT) formalism [55]. To accurately model the structural and electronic properties of the $Cu_2SnS_3$-Cc and $Cu_2SnS_3$-Imm2 phases, we adopted both the generalized gradient approximation (GGA) according to the Perdew-Burke-Ernzerhof (PBE) formalism [56] and the local density approximation (LDA) [57]. To improve the accuracy of describing band gaps and electronic correlation effects, particularly in d orbitals, the modified Tran-Blaha exchange potential (TB-mBJ) was combined with a Hubbard (U) correction (TB-mBJ + U), thereby providing a more accurate representation of electronic interactions in these complex compounds. [58, 59] for all cited systems. In the FP-LAPW method, the Kohn and Sham wave functions are developed in terms of spherical harmonics within the MT spheres for a maximum value of lmax=10.

The muffin-tin sphere radii (Rmt) for $Cu_2SnS_3$-Cc of the Cu, Sn, and S atoms are 2.26 u.a., 2.14 u.a., and 1.95 u.a., respectively; for $Cu_2SnS_3$-Imm2, they are 2.24 u.a., 2.16 u.a., and 1.85 u.a. The size of basis sets was controlled by the parameter RMT. Kmax (where Kmax is the maximum modulus for the reciprocal lattice vector), we have extended the basis function to RMT in our computations. Kmax is equal to 8. The number of k-points in the whole Brillouin zone was chosen as 250 for both systems to converge the total energy, with a mesh of 13×11×13 for the $Cu_2SnS_3$-Ccand and 11×9×11 for the $Cu_2SnS_3$-Imm2 compound. The optical properties of both compounds are calculated using a 1000 k-

point mesh in the irreducible Brillouin zone. The self-consistent iterations are repeated until the convergence energy is less than or equal to $10^{-4}$ Ry.

### 2.2 SCAPS-1D numerical simulation

To design one-dimensional solar cells, we use SCAPS (Solar Cell Capacitance Simulator), a numerical modeling tool provided by the Electronics and Information Systems (ELIS) department at Ghent University, Belgium [60, 61]. Therefore, the software can easily simulate various energy conversion factors, including power conversion efficiency (PCE), fill factor (FF), energy gap (Eg), short-circuit current density (Jsc), quantum efficiency (QE), and current-voltage characteristics (J-V) [62].

Most studies of semiconductor devices are based on the simultaneous solution of Poisson's equation and the continuity equation. It calculates the concentrations of electrons and holes, as well as the value of the electrostatic potential, at every moment and at every point in space using a sequence of finite elements. The relationship between potential and carrier density is expressed by Poisson's equation. [63]:

$$\Delta V = \frac{-q}{\varepsilon}(N_d - N_a + p - n) \tag{1}$$

where V is the potential, q is the elementary charge of electrons, $N_d$ and $N_a$ are the concentrations of ionized donor and acceptor dopants. n and p are the carrier densities. The equations of continuity define the variations in charge density (electrons, holes) and are formulated by the following equations [64]:

$$\frac{\partial n}{\partial t} = G_n - \frac{\Delta n}{\tau_n} + \mu_n\left(\xi\frac{\partial n}{\partial x} + n\frac{\partial \xi}{\partial x}\right) + D_n\frac{\partial^2 n}{\partial^2 x}, \tag{2}$$

$$\frac{\partial p}{\partial t} = G_p - \frac{\Delta p}{\tau_p} + \mu_p\left(\xi\frac{\partial p}{\partial x} + p\frac{\partial \xi}{\partial x}\right) + D_p\frac{\partial^2 p}{\partial^2 x}, \tag{3}$$

where n and p are the concentrations of electrons and holes, $G_n$ and $G_p$ are the electron and hole generation rates, and $\tau_n$ and $\tau_p$ are the electron and hole recombination rates, which themselves have complex expressions related in particular to illumination. The charge carriers can be moved by the presence of both an electric field and a concentration gradient. Under the influence of an electric field, a current called drift current (or conduction current) is generated. This current is proportional to the electric field and defined by the following relationship [65].

$$J_n(x) = q\mu_n nE(x) + qD_n\frac{dn(x)}{dx}, \tag{4}$$

$$J_p(x) = q\mu_p pE(x) + qD_p\frac{dp(x)}{dx}. \tag{5}$$

Here n and p are the concentrations of electrons and holes, $J_n(x)$ and $J_p(x)$ are the electron and hole current densities, where E(x) is the electric field and $\mu_n$ and $\mu_p$ are the mobilities of electrons and holes, respectively.

## 3. RESULTS AND DISCUSSIONS

### 3.1 Structural properties

In this study, the crystal structure of the $Cu_2SnS_3$ compound belongs to the orthorhombic space group (Cc) or monoclinic space group (Imm2), as shown in Figures 1a and 1b. In the unit cell of the CTS compound with the structure, the $Cu^+$ and $Sn^{4+}$ cations occupy distinct sites in the crystal lattice, while the $S^{2-}$ anions provide the bond between these tetrahedral units. This phase is less common than the monoclinic and cubic phases, whereas in monoclinic CTS, Cu and Sn atoms completely occupy the two separate tetrahedral sites in an orderly manner at the cation positions and do not share the same atomic positions and are distorted with different M-S distances.

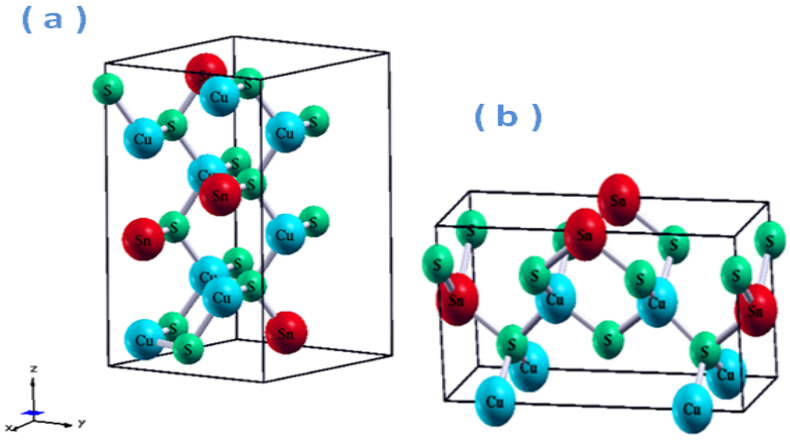


**Figure 1.** The crystal structure of $Cu_2SnS_3$ compounds: (a): Monoclinic with Cc symmetry, (b): Orthorhombic with Imm2 symmetry

In the current structural optimization, we aim to determine the ground state of our compound, which was initially required. More than a hundred iterations of the process were done until the total energy calculation converged. The parameters of the network at equilibrium are calculated by adjusting the total energy of the volume using Murnaghan's empirical formula [66], following the well-known relationship:

$$E(V) = E_0 + \left[\frac{B_0 V}{B'(B'-1)}\right].\left[B'\left(1-\frac{V_0}{V}\right) + \left(\frac{V_0}{V}\right)^{B'} - 1\right], \quad (6)$$

where B and B' denote the compression modulus and its derivative, respectively. $V_0$ is the volume of the ground state. The modulus of compressibility (B) and its derivative ($B_0'$) are defined by:

$$B_0 = V\left(\frac{\partial^2 E}{\partial V^2}\right), \quad (7)$$

$$k = \frac{\partial B}{\partial P}. \quad (8)$$

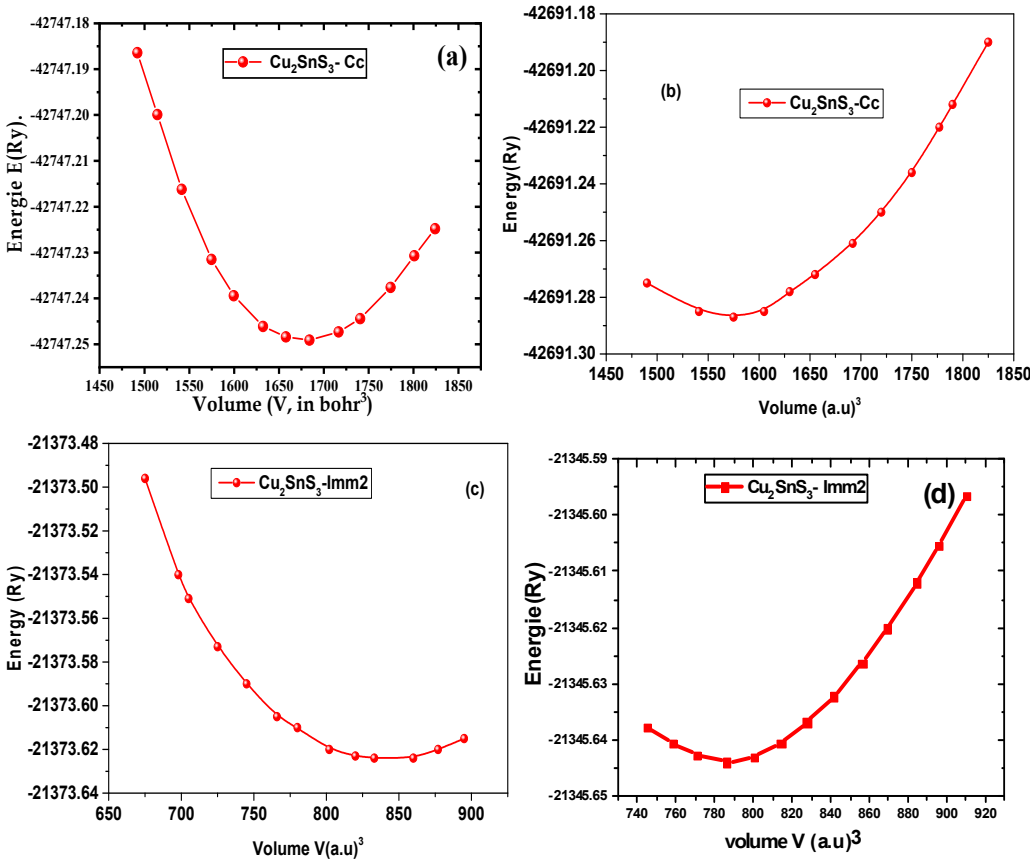


**Figure 2.** Volume optimization of $Cu_2SnS_3$-Cc was performed using (a) GGA-PBE and (b) LDA, while $Cu_2SnS_3$-Imm2 was optimized using (c) GGA-PBE and (d) LDA approximations

As illustrated in Figures 2a, b, c, and d, the predicted variation of the total energy versus the cell volume for $Cu_2SnS_3$-Cc and $Cu_2SnS_3$-Imm2 using both well-known exchange and correlation LDA and GGA-PBE functionals. All the obtained results, such as (lattice constants a, bulk modulus B, and its derivative B'), are obtained using the plane wave method and the pseudo potentials are summarized in the Table. 1. One could observe easily that the obtained results according to the GGA functional are the closest ones with an excellent correlation to the experimental counterpart [67-69].

**Table 1.** Calculated lattices constants (a, b, c) in (Å), bulk modulus *B* (GPa), the derivative and *β* (Deg), of $Cu_2SnS_3$-Cc and $Cu_2SnS_3$-Imm2

| | a(Å) | b(Å) | c(Å) | B (GPa) | B ′ | β (Deg) |
|---|---|---|---|---|---|---|
| | $Cu_2SnS_3$-Cc | | | | | |
| **LDA** | 6.59* | 11.41* | 6.62* | 90.67* | 4.94* | 111.07* |
| **GGA** | 6.70* | 11.67* | 6.73* | 68.70* | 4.85* | 109.37* |
| **Other Calcul** | 6.65[a],<br>6.654[b]<br>6.653[c]<br>6.71[d] | 11.54[a],<br>11.534[b]<br>11.536[c]<br>11.620[d] | 6.67[a],<br>6.654[b]<br>6.665[c]<br>6.74[d] | -<br>-<br>-<br>- | -<br>-<br>-<br>- | 109.39[a, c],<br>109.67[d]<br>-<br>- |

| | a(Å) | b(Å) | c(Å) | B (GPa) | B ′ | β (Deg) |
|---|---|---|---|---|---|---|
| | $Cu_2SnS_3$-Cc | | | | | |
| | 6.079[e] | | 6.741[e] | - | - | - |
| | $Cu_2SnS_3$-Imm2 | | | | | |
| **LDA** | 3.76* | 5.18* | 11.24* | 91.48* | 5.52* | - |
| **GGA** | 3.91* | 5.42* | 11.65 | 71.46* | 4.47* | - |
| **Other Calcul** | 3.92[d]<br>3.923[e] | 5.43[d]<br>5.428 [e] | 11.61[d]<br>11.612[e] | -<br>- | -<br>- | -<br>- |

*Present calculations, [a]Ref [67] Experimental (photoreflectance spectroscopy (PR), [b]Ref [68] Experimental, [c]Ref [69] X-ray diffraction method, [d]Ref [50] PBE-GGA and TB-mBJ approximations, [e]Ref [70] TB-mBJ approach and Hubbard potential.

The comparative study is well elucidated in the Table. 1 of the obtained results enables us to employ the PBE-GGA approximation as the practical potential, based on rigorous crystallographic atomic positions, thereby providing our study with an accurate electronic band-gap configuration.

## 3.2 Electronic properties

### 3.2.1 Band structure

Based on equilibrium structural parameters for the $Cu_2SnS_3$-Cc and $Cu_2SnS_3$-Imm2 structures, we investigate the electronic characteristics of $Cu_2SnS_3$ compounds. We use the modified Becke Johnson potential (mBJ), the Hubbard formalism (U), and the generalized gradient approximation (PBE-GGA). The Fermi level is referenced at 0 eV. We compute the band structures for our compounds along the directions of symmetry in the first zone of Brillouin (ZB).

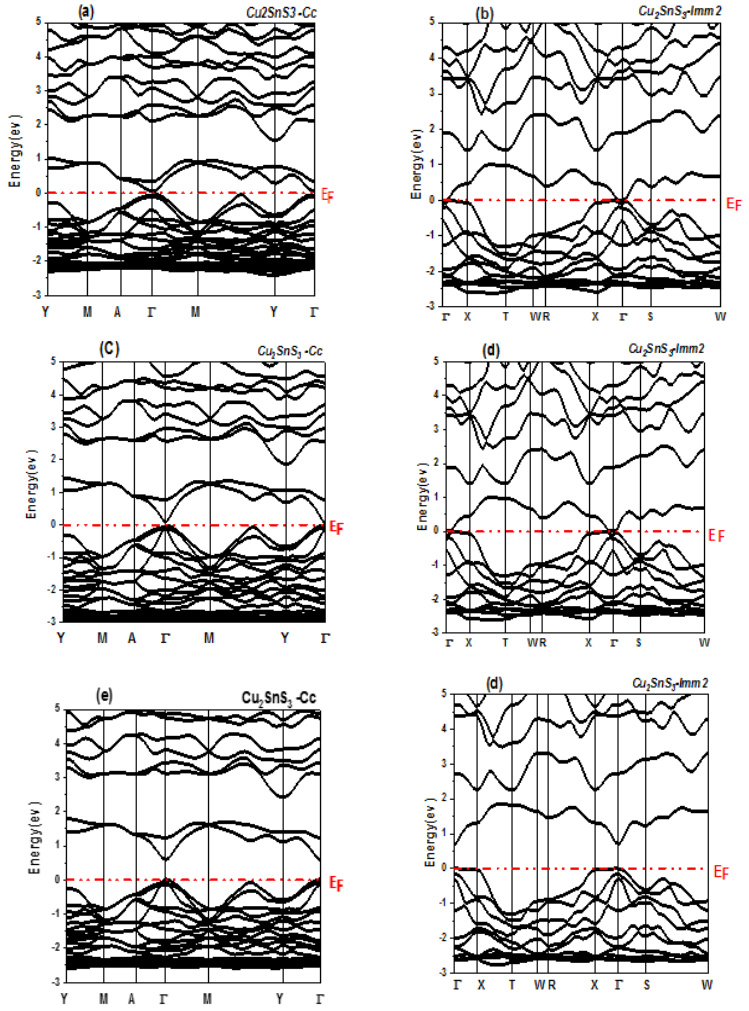


**Figure 3.** The band structures of $Cu_2SnS_3$ in the Cc phase (left panel) were computed using: (a) PBE-GGA, (c) Hubbard correction, and (e) TB-mBJ+U, while those of $Cu_2SnS_3$ in the Imm2 phase (right panel) were obtained using: (b) PBE-GGA, (d) Hubbard correction, and (f) TB-mBJ+U

Initially, we employed the GGA approximation to calculate the band gap, which revealed that the CTS material is a metal, as illustrated in Figs. 3(a) and 3 (b). We note a gap of 0.086 eV for $Cu_2SnS_3$-Cc-Cc and 0 eV for $Cu_2SnS_3$-Imm2 at the high symmetry point *Γ*. By comparing our results with the experimental value of 0.92 eV for the monoclinic phase [71, 72], we note a significant discrepancy. For the d-type orbital correction on Cu atoms, we employed the TB-mBJ + U

approximation [73], which accounts for the overlap involving the Cu 3d orbitals that constitute the top of the valence band." To determine the correct Ud (Cu) value, we conducted a series of tests, as shown in Table 2, and recorded the resulting values. Through these tests, we established that Ud (Cu) = 6 eV is the appropriate value to correct this situation.

**Table 2** Band gap calculation of $Cu_2SnS_3$

| Compound | Energy gap Eg (eV) | | | | | | | | | |
|---|---|---|---|---|---|---|---|---|---|---|
| | GGA | Hubbard | | | | TB-mbj +U | | | | Other Calaculations |
| | | $U_d$=0 | $U_d$=2 | $U_d$=4 | $U_d$=6 | $U_d$=0 | $U_d$=2 | $U_d$=4 | $U_d$=6 | |
| **$Cu_2SnS_3$-Cc** | 0.086 | 0.086 | 0.13 | 0.19 | 0.26 | 0.29 | 0.36 | 0.52 | 0.70 | 0.70[70],0.88[74] 0.95[75] |
| **$Cu_2SnS_3$-Imm2** | 0 | - | - | - | .0065 | - | - | - | 0.73 | 0.60[70] |

The obtained electronic band structures of $Cu_2SnS_3$-Cc and $Cu_2SnS_3$-Imm2 structures are shown in Fig. 3 (c, d, e, and f). It is clear that both compounds exhibit p-type semiconductors with direct band gaps (Γ–Γ) of 0.70 eV for $Cu_2SnS_3$-Cc and 0.732 eV for $Cu_2SnS_3$-Imm2. The results obtained are consistent with previously reported experimental values. The band gap, as determined by the various approximations employed in this section, is summarized in Table 2.

### 3.2.2 Density of state

To elucidate the orbital hybridization mechanisms in CTS alloys and clarify the contributions of different atomic states to the electronic band structures, the predicted total density of states (TDOS) and partial density of states (PDOS) were calculated and are shown in Figs. (4a) and (4b), respectively. The Fermi level (EF) was arbitrarily set at 0 eV to serve as an energy reference. We note that there is a similarity in density of states to monoclinic and orthorhombic structures of $Cu_2SnS_3$, where we find that the energy region between [-14, -6] eV.

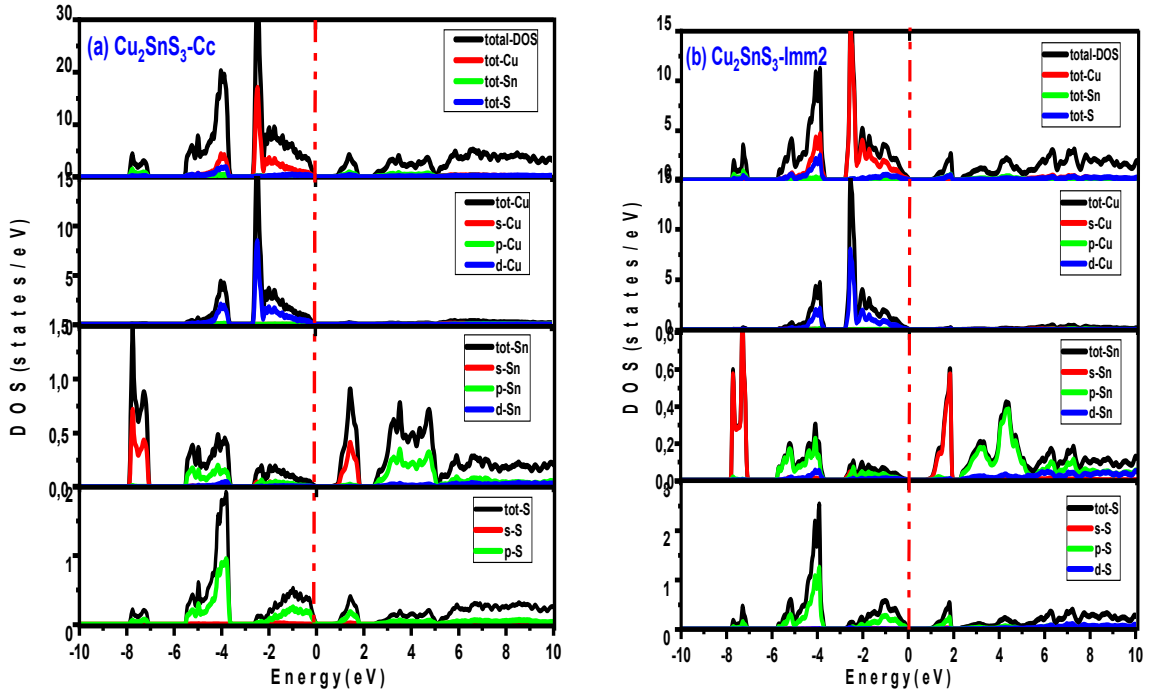


**Figure 4.** The density of states (DOS) partial and total of $Cu_2SnS_3$-Cc and $Cu_2SnS_3$-Imm2 using (GGA-PBE)

The electronic states corresponding to the s and p orbitals of the Sn atom, as well as the s orbitals of the S atom, are confined to an energy band located approximately between -14 eV and -6 eV. The failure of the PBE-GGA approximation to calculate the band gap is further exacerbated by the observation that the conduction band around the Fermi level is primarily composed of Cu (d) with a minor contribution from the p states of (Sn) and (S). The d states of Cu predominate at the maximum of the valence band.

The energy region [0,14] eV is characterized by the significant contribution of the p of (Sn) and the small contribution of the p of (S), which resulted in a gap of 0.7 and 0.73 electron-volts for $Cu_2SnS_3$-Cc and $Cu_2SnS_3$-Imm2, respectively. Eventually, the $Cu_2SnS_3$ compound exhibits semiconductor behavior; this property likely makes it a promising candidate for various applications.

### 3.3 Optical Properties

The optical properties of solids for the complete range of photon energies can be characterized as the complex dielectric function, defined by the following formula [76]:

$$\varepsilon(\omega) = \varepsilon_1(\omega) + i\varepsilon_2(\omega). \quad (9)$$

The imaginary component $\varepsilon_2(\omega)$ of the dielectric function, at a given angular frequency ω, is determined from the sum of the contributions of all possible electronic transitions between occupied and unoccupied states. It is expressed by the following relation: [77, 78]:

$$\varepsilon_2(\omega) = \frac{8}{3\pi\omega^2}\sum_{ij}\int\left|P_{ij}(k)\right|^2 \frac{dS_k}{\nabla\omega_{ij}(k)}, \tag{10}$$

Where $P_{ij}(k)$ represent the components of the dipole moment matrix between $|nk\rangle$and $|\dot{n}k\rangle$

The indices i and j represent the initial and final states of the system, respectively, and are used to identify the configurations before and after the transition in question. Indeed, the real part of the dielectric function is given by the Kramers-Kronig and can be expressed as [78, 79]:

$$\varepsilon_1(\omega) = 1 + \frac{2}{\pi}P\int_0^{\infty}\frac{\varepsilon_2(\omega')\omega' d\omega'}{\omega'^2-\omega^2}, \tag{11}$$

where *P* the principal part of the Cauchy integral and ω is the frequency. It is possible to use the complex dielectric tensor to calculate various optical constants, such as the refraction coefficient $n(k)$ and the extinction coefficient $k(\omega)$ which are given by the equation:

$$n(\omega) = \frac{1}{\sqrt{2}}[(\varepsilon_1{}^2(\omega) + \varepsilon_2{}^2(\omega))^{\frac{1}{2}} + \varepsilon_1(\omega)]^{1/2}, \tag{12}$$

$$K(\omega) = \frac{1}{\sqrt{2}}[(\varepsilon_1{}^2(\omega) + \varepsilon_2{}^2(\omega))^{\frac{1}{2}} - \varepsilon_1(\omega)]^{1/2}. \tag{13}$$

Other very interesting optical grades that can be deduced from the complex index are the reflection coefficient R and the absorption coefficient $\alpha(\omega)$, which can be expressed by [80]

$$\mathrm{Re}\,\sigma(\omega) = \frac{\omega}{4\pi}\mathrm{Im}\,\varepsilon(\omega), \tag{14}$$

$$\alpha(\omega)\frac{4\pi}{\lambda}\mathrm{k}(\omega). \tag{15}$$

Studying the optical properties of materials allows us to know the way they interact with light as well as their electrical structure in order to know the possibility of their application in the field of optoelectronic applications. In this section, we will investigate the optical properties of the compound $Cu_2SnS_3$ in its various phases, focusing on key parameters such as the absorption coefficient and refractive index. This analysis aims to describe electronic transitions and vibrations, particularly in the visible, ultraviolet, and infrared regions.

### 3.3.1 Dielectric function

For $Cu_2SnS_3$ in both the Cc (red curve) and Imm2 (blue curve) crystal phases, Fig. 5(a) shows the real component of the dielectric function, $\varepsilon_1(\omega)$, and Fig. 5(b) the imaginary part, $\varepsilon_2(\omega)$. The material's dispersion and polarization behavior can be inferred from the $\varepsilon_1(\omega)$ spectrum. Both phases exhibit positive $\varepsilon_1(\omega)$ values in the visible and near-infrared regions (up to ~3.3 eV), which is favorable for optoelectronic applications, as it indicates low absorption and strong dielectric transparency. In the Cc phase, we observe a sharp peak at approximately 5 eV, which can be attributed to the increased polarization of the UV spectrum. However, at high photon energy, where it exceeds 8 eV, the values become negative, and this compound has a reflective property similar to metals.

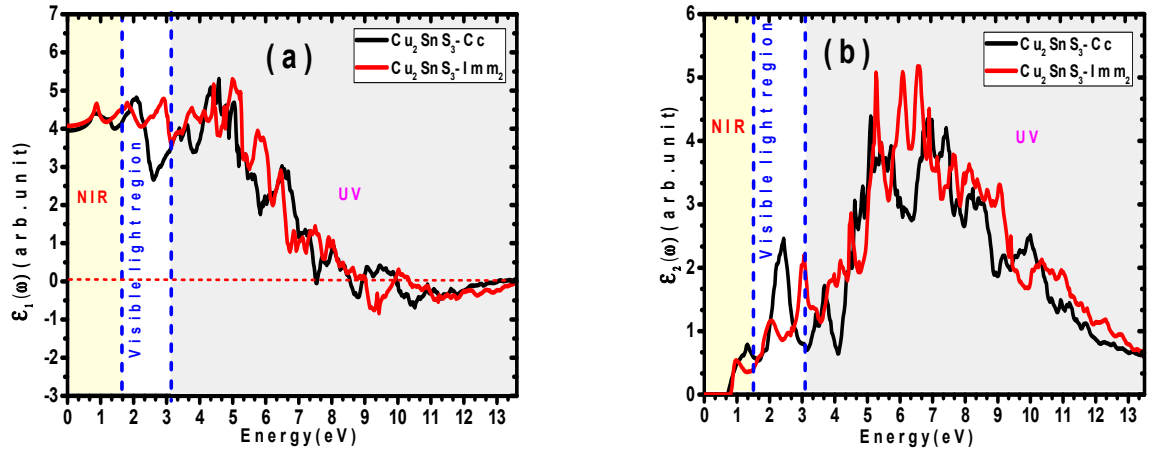


**Figure 5.** Dielectric function: Real part (a) and Imaginary part (b) of $Cu_2SnS_3$ in the Cc and Imm2 phases calculated using the TB-mBJ+U method

As for the optical absorption properties related to interband electronic transitions, they are visualized by the $\varepsilon_2(\omega)$ spectrum in Fig. 5(b). There is a great similarity between the spectra in the two phases, with the $\varepsilon_2(\omega)$ values of the Imm2 phase usually appearing at slightly larger values. The onset of absorption (first non-zero $\varepsilon_2$ values) occurs at about 1 eV, which means a comparable band gap. It also includes many peaks between 3 and 8 eV, indicating excellent absorption properties in the UV spectrum, which means more effective absorption of photons. This feature allows use in the field of photocatalysis and photovoltaic applications.

Ultimately, it can be said that the $Cu_2SnS_3$ compound is a good absorber of UV-visible, as both phases exhibit unique dielectric responses. These discoveries open up new possibilities for designing materials with adjustable optical properties that can be utilized in optoelectronic devices and solar energy conversion applications.

### 3.3.2 Absorption coefficient, reflectivity, refraxion and extinction index

The absorption coefficient enables us to describe a material's ability to absorb incident photons, thereby evaluating its performance in optoelectronic and photovoltaic applications. The optical absorption coefficient of $Cu_2SnS_3$ for the Cc (red curve) and Imm2 (blue curve) crystal structures is shown in Fig. 6 (a) as a function of photon energy. As the photon energy moves into the visible and ultraviolet (UV) ranges, both phases show a dramatic rise in absorption, which is negligible in the near-infrared region (below ~1.5 eV).

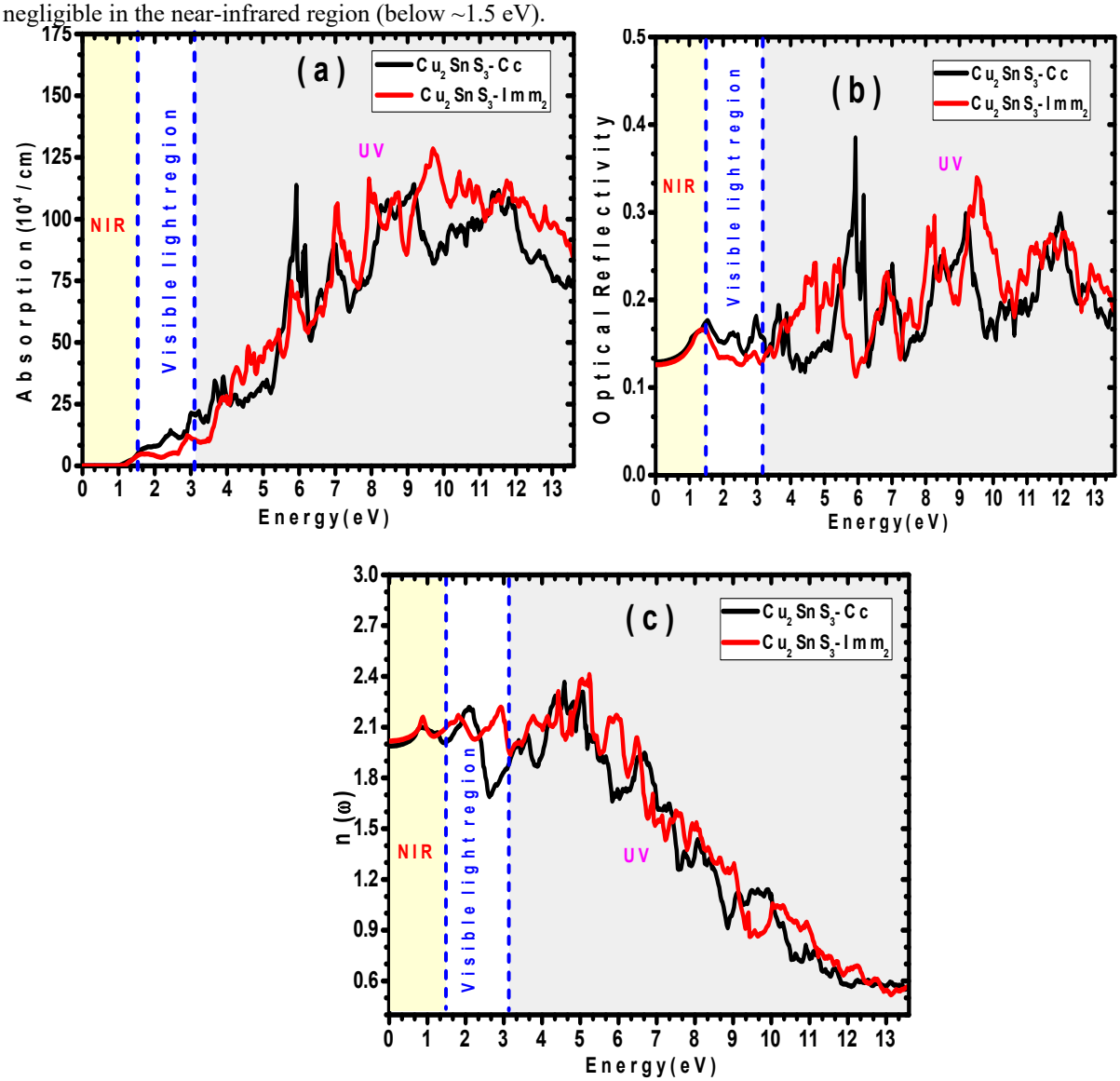


**Figure 6.** Absorption coefficient (a), reflectivity (b) and refraxion(c) of $Cu_2SnS_3$-Cc and $Cu_2SnS_3$-Imm2 using TB-mBJ+U

There is a comparable band gap, as evidenced by the onset of absorption at 1 eV. Both structures also show significant absorption accompanied by prominent peaks in the UV region, reaching limit values above $10^5$ $cm^{-1}$. This suggests that there are numerous permitted electronic transitions. In the region of 8–11 eV, the Cc phase exhibits somewhat greater absorption values compared to the Imm2 phase, indicating a stronger interaction with high-energy photons.

Optical reflectivity indicates the amount of incident light reflected from the surface of a material. It is an important metric for applications such as sensors, photovoltaics, and optical coatings. We plotted the optical reflectivity of $Cu_2SnS_3$ in the Cc (red line) and Imm2 (blue line) phases against photon energy in Fig. 6 (b). Both phases show comparatively low reflectivity, typically below 0.2, in the visible and near-infrared ranges (0–3.3 eV), suggesting that the majority of incident light in this range is either absorbed or transmitted. This is a beneficial characteristic for light-harvesting devices such as solar cells. Reflectivity rises and exhibits multiple noticeable oscillations that correspond to interband transitions as photon energy increases into the ultraviolet (UV) range. The Imm2 phase shows somewhat higher and more variable reflectance values in the UV spectrum, especially between 5 and 8 eV, due to its unique electronic band structure. As for the Cc phase, the reflectivity remains relatively smoother.

The graph with the sign 6 (c) expresses the change in the refractive index value of the $Cu_2SnS_3$ compound in its $Cu_2SnS_3$-Cc and $Cu_2SnS_3$-Imm2 phases across the spectra of visible light, ultraviolet, and near-infrared light spectrums. Both phases exhibit comparable and consistent refractive indices (1.8-2.1) in the near infrared. The index rises for both in the visible zone. The refractive index exhibits more intricate behavior in the UV spectrum, with peaks and valleys that correspond to different electronic transitions. Interestingly, $Cu_2SnS_3$-Cc typically exhibits sharper features and significantly higher indices in the 3.0-6.0 eV range, indicating variations in its optical sensitivity to higher-energy photons.

### 3.4 Numerical device modelling

The one-dimensional software SCAPS-1D allows the modeling of any photovoltaic structure using the materials listed in its data files, while offering the possibility of modifying various parameters, such as layer thickness, surface area, and doping level. This simulator relies on an iterative and self-consistent numerical solution of a system of coupled differential equations, including Poisson and continuity equations for majority and minority carriers (electrons and holes), in order to predict the electrical behavior and performance of photovoltaic devices [81].

The structure analyzed is a planar configuration shown in Fig. 7, consisting of an n-type indium gallium zinc oxide (IGZO) layer, which serves as both the electron transport layer (ETL) and the front contact (anode). It also incorporates p-type material ($CuSnS_3$), used as an absorbing material, as well as different materials placed as p-type layers that act as hole transport material (HTL) to the gold (Au) metal electrode, such as $Cu_2O$, which is known for its wide bandgap, giving it transparency in the visible spectrum. P3HT is an organic conductor sensitive to visible light. DPBTTT-14 is commonly used as a hole transport material (HTM) due to its superior electrical conductivity and high charge carrier mobility.

The studied structure is a planar structure with the configuration FTO/$CuSnS_3$/HTL, as shown in Fig 7. The simulation was performed under standard conditions, with lighting of 1000 W/m² at 300 K and an air mass of AM 1.5G. The simulation was performed using parameters specific to each material purposes are listed in Table 3.

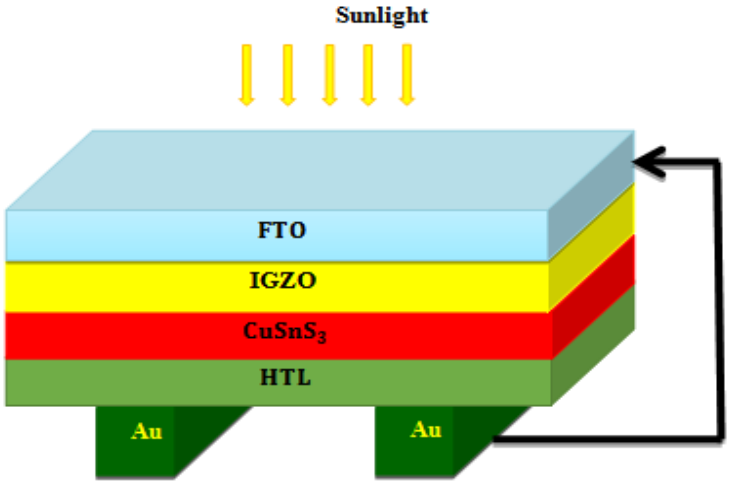


**Figure 7.** Architecture of the primary p-i-n type perovskite solar cell device

**Table 3.** The parameters for each material were used for simulation.

| Parameters | FTO [76] | IGZO [77] | $Cu_2SnS_3$ | $Cu_2O$ [78] | D-PBTTT-14 [78] | P3HT [79] |
|---|---|---|---|---|---|---|
| **Eg (eV)** | 3.5 | 3.05 | 0.88 | 2.17 | 2.16 | 2 |
| **χ, (eV)** | 4 | 4.16 | 3.9 - 4.3 | 3.2 | 3.2 | 3.2 |
| **Ɛ** | 9 | 10 | $10^{-20}$ | 7.11 | 10 | 3 |
| **Nc ($cm^{-3}$)** | $2.2\times10^{18}$ | $5\times10^{18}$ | $2.2\times10^{18}$ | $2.02\times10^{17}$ | $2.8\times10^{19}$ | $10^{20}$ |
| **Nv ($cm^{-3}$)** | $1.8\times10^{19}$ | $5\times10^{18}$ | $2.9\times10^{18}$ | $1.1\times10^{19}$ | $2.5\times10^{21}$ | $10^{20}$ |
| **$\mu_n$ ($cm^2$ $V^{-1}$ $s^{-1}$)** | 20 | 15 | $10^1$ - $10^3$ | 200 | $10^{-4}$ | $10^{-4}$ |

| Parameters | FTO [76] | IGZO [77] | $Cu_2SnS_3$ | $Cu_2O$ [78] | D-PBTTT-14 [78] | P3HT [79] |
|---|---|---|---|---|---|---|
| $\mu_h$ ($cm^2 V^{-1} s^{-1}$) | 10 | 0.1 | 10 - 100 | 80 | $10^{-4}$ | $10^{-4}$ |
| ND ($cm^{-3}$) | $2\times10^{19}$ | $10^{18}$ | $10^{16}$ - $10^{19}$ | 0.0 | 0.0 | 0.0 |
| NA ($cm^{-3}$) | 0.0 | 0.0 | $10^{18}$ - $10^{20}$ | $10^{18}$ | $10^{18}$ | $10^{16}$ |
| Nt($cm^{-3}$) | $10^{15}$ | $2.0\times10^{15}$ | $10^{14}$ | $10^{14}$ | $10^{14}$ | $10^{15}$ |

### 3.4.1 Influence of ETL materials

We modified the hole transport layer (HTL) in this cell and analyzed the impact of different hole transport materials on the current-voltage ($J_V$) properties using IGZO as the electron transport layer (ETL). Show Table 4. According to these results, PSCs with a $Cu_2O$ HTL have the best energy conversion efficiency (PCE). Thedifferenceof bandgap between perovskite and the $Cu_2O$ layer is significant; however, it is possible to achieve high conversion efficiency ($P_{CE}$) through effective contact between the active layer and the metal electrode.

**Table 4.** Comparative analysis of hole transport materials in structures incorporating IGZO as the ETL layer.

| | $Cu_2O$ | P3HT | D-PBTTT-14 |
|---|---|---|---|
| Voc (V) | 0.833 | 0.824 | 0.831 |
| Jsc ($mA/cm^2$) | 49.44 | 94,44 | 49,44 |
| FF (%) | 84.40 | 79 .05 | 84.36 |
| PCE (%) | 34.79 | 32 ,21 | 34.68 |

### 3.4.2 Influence of absorbing layer thickness

The absorber layer plays a crucial role in the cell's performance [82]. To achieve this role, we will vary the absorber layer thickness from 100 nm to 800 nm. The simulation results are shown in Fig. 8. We can see that the variation in the thickness of the $CuSnS_3$ affects all the parameters of the cell. The current density Jsc increases with the increase in the thickness of the absorber ($CuSnS_3$), which is due to the latter's high absorption coefficient. For the others, an increase in the form factor, especially for $Cu_2O$, justifies the latter as a candidate promoter in this device. This simulation study, therefore, confirms that the film must have an optimal thickness of 800 nm. This demonstrates that perovskite is a material capable of achieving better light absorption and higher efficiency, even with thicknesses of a few hundred nanometers.

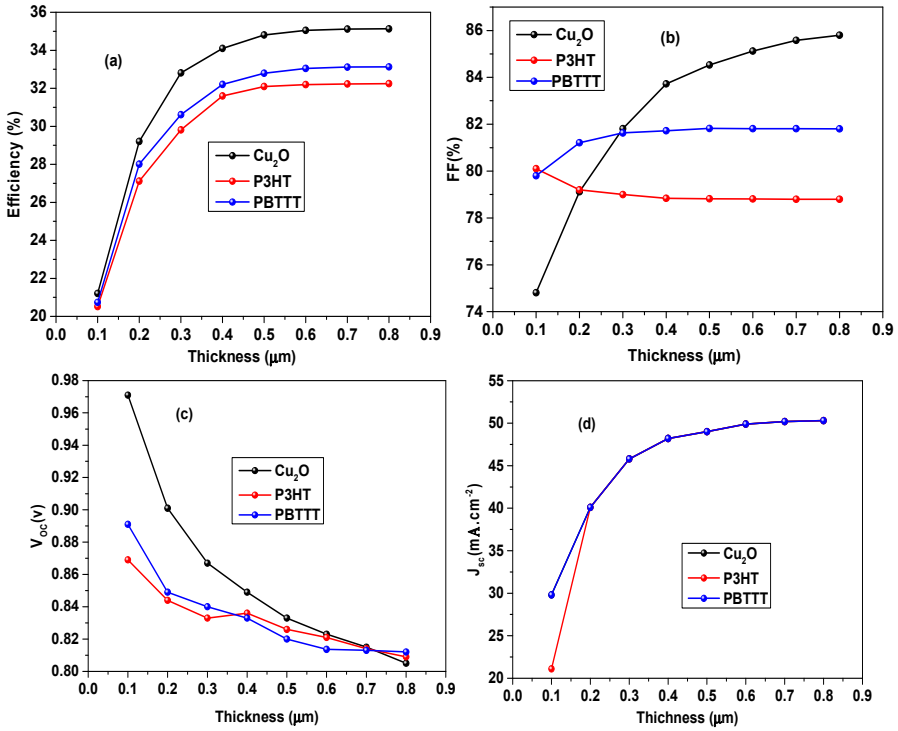


**Figure 8.** Variation of photovoltaic parameters as a function of the thickness of $Cu_2SnS_3$: a) Conversion efficiency ($P_{CE}$), b) Fill factor (FF), c) Open-circuit voltage ($V_{oc}$), and d) Short-circuit current density ($J_{sc}$)

### 3.4.3 Effect of Doping on Various Device Components

Doping plays a crucial role in the performance variations of solar cells, as it directly influences the electrical properties of different regions of the device and allows for the optimization of charge carrier generation and collection [83,84]. In this section, we propose a study of optimal properties for the active layer and observe that the impact of doping absorbers with p-type carriers manifests itself in a range from $10^{12}$ to $10^{21}$ $cm^{-3}$, as illustrated in Fig. 9.

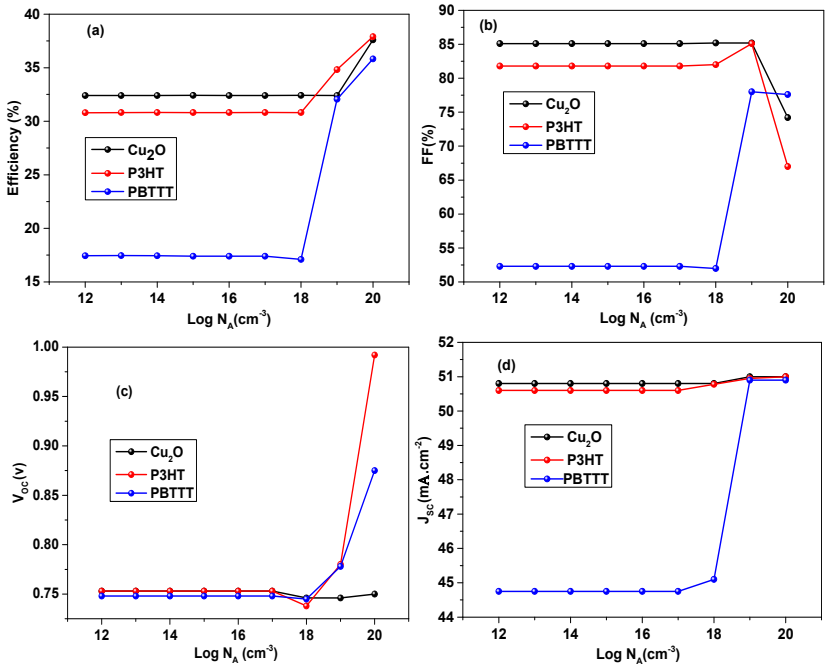


**Figure 9.** Impact of doping on variations in solar cell performance: a) PCE, b) FF, c) $V_{OC}$ and d) $J_{sc}$

The results reveal that efficiency increases with dopant concentration up to $10^{20}$ $cm^{-3}$. Notably, in the cases of $P_3HT$ and $Cu_2O$, the values reach 37.85% and 37.3%, respectively. The fill factor (FF) increases slightly to $10^{19}$ $cm^{-3}$ for D-PBTTT-14, while for $P_3HT$ and $Cu_2O$, it remains almost constant at $10^{19}$ $cm^{-3}$, then decreases sharply beyond this doping density. As $N_A$ increases, the Fermi energy level of the holes approaches the valence band (VB), resulting in an increase or constancy of $V_{OC}$ and $J_{SC}$.

The stability in $J_{SC}$ for solar cells with $Cu_2O$ and $P_3HT$ as HTLs, for D-PBTTT-14, exhibits a crossover up to $10^{20}cm^{-3}$. The $V_{OC}$ is stable between $10^{12}$ and $10^{18}$ $cm^{-3}$, then increases for HTL P3HT and D-PBTTT-14, and remains stable for HTL $Cu_2O$. This indicates that a higher dopant concentration was ineffective and led to deep defects.

### 3.4.4 Effect of External Operating Temperature

The performance of solar cells is significantly affected by operating temperature [85]. We utilized the SCAPS-1D solar cell simulator to investigate the temperature-dependent variability in the device's performance. 300 K to 400 K, in 10°C increments, under standard 1 sun illumination conditions, as described in our previous work [80].

As shown in Fig. 10, both the fill factor (FF) and the power conversion efficiency ($P_{CE}$) of the hole transport layer decrease as temperature increases. According to Equation 16, this behavior is attributed to the temperature-dependent rise in the dark saturation current ($J_0$). This leads to a decrease in open-circuit voltage ($V_{OC}$). This finding corresponds well with our simulation results.

$$V_{OC} = \frac{AKT}{e} Ln\left[\frac{J_{ph}}{J_0} + 1\right]. \quad (16)$$

Furthermore, as temperatures rise, internal resistance decreases due to the low resistivity of the materials. This promotes better current flow, which reduces energy losses and increases the fill factor (FF).

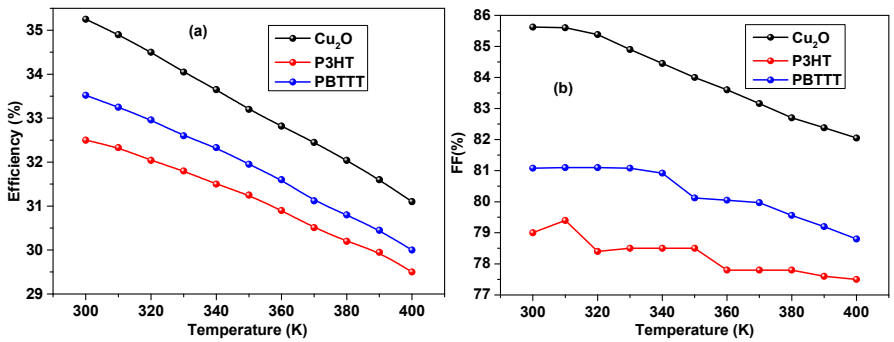


**Figure 10.** Influence of operating temperature on the performance parameters of solar cells, namely: (a) power conversion efficiency (PCE), (b) fill factor (FF), (c) open-circuit voltage (Voc), and (d) short-circuit current density (Jsc)

(*continued on next page*)

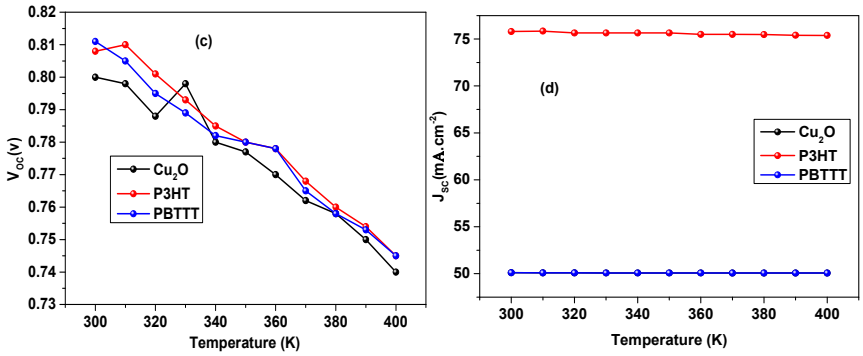


**Figure 10.** Influence of operating temperature on the performance parameters of solar cells, namely: (a) power conversion efficiency (PCE), (b) fill factor (FF), (c) open-circuit voltage (Voc), and (d) short-circuit current density (Jsc)

## 5. CONCLUSIONS

This work has enabled the achievement of the objectives set for studying the structural, optoelectronic, and photovoltaic performance of the $Cu_2SnS_3$ compound, through a combined simulation process based on density functional theory (DFT) and the SCAPS-1D software. A comparative analysis of the structural, electronic, and optical properties of CTS ($Cu_2SnS_3$) was performed to evaluate its potential for photovoltaic applications. Our calculations were performed using direct LDA (or GGA) methods, but the values obtained suggested that the compound $Cu_2SnS_3$ is a metal, contrary to what experimental studies have demonstrated. This is because this type of semiconductor is based on copper. We note that the Cud electrons possess a dual nature, enabling them to hybridize with Sn *s* electrons. Therefore, this compound appeared to be metallic in nature. In order to displace the anion, The TB-mBJ+U functional, which combines the Tran and Blaha modified Becke–Johnson potential with a Hubbard U term, was introduced to better account for electron correlation effects, as the results were largely consistent with the experiment, as both structures, Cc and Imm2, appeared as p-type semiconductors with direct gaps ($\Gamma$-$\Gamma$) of 0.7 eV and 0.7 eV, respectively. Regarding the study of optical properties, the compound $Cu_2SnS_3$ exhibits increased polarization in the ultraviolet spectrum at high photon energies in both phases. It is also characterized by positive $\varepsilon_1(\omega)$ values up to 3 eV, making this compound, in both phases, a candidate for electronic applications. In the last part of this work, we proved the effectiveness of the $Cu_2SnS_3$ compound in the field of photovoltaic cells, where, using the SCAPS program, we took this compound as an absorption layer, where the simulation showed that the current density Jsc increases even to its peak, which leads to an increase in the absorption coefficient, and this is at a thickness of 800 nanometers. Several questions remain to be explored to fully understand how structural, optoelectronic, and photovoltaic properties influence the behavior of the $Cu_2SnS_3$ compound. The results presented in this study make a significant contribution to this understanding and provide valuable insights for the development of high-performance materials for solar energy.

## ORCID

**Boualem Kada,** https://orcid.org/0009-0007-2817-4167; **Benyahia Karima,** https://orcid.org/0000-0001-8690-8949
**Beloufa Nabil,** https://orcid.org/0009-0004-8612-3948; **Hamza Rekab Djabri,** https://orcid.org/0000-0002-2458-1335
**Djamel Eddine Belfennache**, https://orcid.org/0000-0002-4908-6058; **Alami Ahmed,** https://orcid.org/0000-0001-7000-8292
**Hamad M. Adress Hasan,** https://orcid.org/0000-0002-6739-8311

## REFERENCES

[1] R. Ouldamer, D. Madi, and D. Belfennache, in: *Advanced Computational Techniques for Renewable Energy Systems. IC-AIRES 2022. Lecture Notes in Networks and Systems*, vol. 591, edited by M. Hatti, (Springer, Cham. 2023). pp. 700-705, https://doi.org/10.1007/978-3-031-21216-1_71
[2] S. Mahdid, D. Belfennache, D. Madi, M. Samah, R. Yekhlef, and Y. Benkrima, J. Ovonic. Res. **19**(5), 535-545 (2023). https://doi.org/10.15251/JOR.2023.195.535
[3] D. Belfennache, N. Brihi, and D. Madi, in: *Proceedings of the IEEE xplore, 8th (ICMIC)* (IEEE, 2017). pp. 497–502. https://doi.org/10.1109/ICMIC.2016.7804164
[4] A.C. Lokhande, P.T. Babar, V.C. Karade, M.G. Gang, V.C. Lokhande, C.D. Lokhande, and J.H. Kim, J. Mater. Chem. A, **7**, 17118–17182 (2019). https://doi.org/10.1039/C9TA00867E
[5] C. Xing, Y. Lei, M. Liu, S. Wu, W. He, and Z. Zheng, Phys. Chem. Chem. Phys. **23**, 16469 (2021). https://doi.org/10.1039/D1CP02067F
[6] F. Saker, L. Remache, D. Belfennache, K.R. Chebouki, and R. Yekhlef, Chalcogenide Lett. **22**(2), 151 (2025). https://doi.org/10.15251/CL.2025.222.151
[7] Q. Zhao, R. Han, A.R. Marshall, S. Wang, B.M. Wieliczka, J. Ni, J. Zhang, *et al*., Adv Mater. **34**, 2107888 (2022). https://doi.org/10.1002/adma.202107888
[8] F. A. Boukhelkhal, N. Selmane, A. Cheknane, M. Noureddine, A. Zoukel, N. Baydogan, B. Günalan, and H. S. Hilal, Chem. Phys., **601**,112952 (2026), https://doi.org/10.1016/j.chemphys.2025.112952
[9] A. Saoudi, Y. Bouznit, F. Chouikh, and G. Leroy, Chem. Phys. **600**, 112894 (2026). https://doi.org/10.1016/j.chemphys.2025.112894

[10] J. Chi, H. Wei, L. Chu, L. Han, T. Liu, X. Zhong, D. Kou, *et al*., Energy Environ. Sci. **18**, 8366 (2025). https://doi.org/10.1039/D5EE02706C
[11] S. Tao, H. Wang, M. Jia, J. Han, Z. Wu, J. Zhou, M. Baranova, *et al*., Adv. Funct. Mater. **35**(23), 2423251 (2025). https://doi.org/10.1002/adfm.202423251
[12] P.A. Fernandes, P.M.P. Salomé, and A.F. Da Cunha, J. Phys. D: Appl. Phys. **43**, 215403 (2010). https://doi.org/10.1088/0022-3727/43/21/215403
[13] A.G. Chronis, E. Karantagli, F.I. Michos, C.S. Garoufalis, and M.M. Sigalas, Solid. State. Commun. **332**, 114326 (2021). https://doi.org/10.1016/j.ssc.2021.114326
[14] X. Wu, Z. Zhang, and H. Soleymanabadi, Solid. State. Commun. **306**, 11377 (2020). https://doi. /10.1016/j.ssc.2019.113770
[15] E.J. Skoug, J.D. Cain, D.T. Morelli, J. Alloys. Compd. **506**, 18 (2010). https://doi.org/10.1016/j.jallcom.2010.06.182
[16] L.K. Samanta, Phys. Status Solidi a, **100**, K93 (1987). https://doi.org/10.1002/pssa.2211000165
[17] G. Marcano, C. Rincon, L.M. De Chalbaud, D.B. Bracho, and G.S. Perez, J. Appl. Phys. **90**, 1847 (2001). https://doi.org/10.1063/1.1383984
[18] S.K. Biswas, M.M. Ahmed, M.F. Orthe, M.S. Sumon, and K. Sarker, Eur. J. Electr. Eng. Comput. Sci. **7**, 63 (2023). https://doi.org/10.24018/ejece.2023.7.5.558
[19] P.P.J. Helan, K. Mohanraj, G. Sivakumar, Iran. J. Sci. Technol. Trans. A Sci. **42**, 1677 (2018). https://doi.org/10.1007/s40995-017-0355-1
[20] G.H. Chandra, O.L. Kumar, R.P. Rao, and S. Uthanna, J. Mater. Sci. **46**, 6952 (2011). https://doi.org/10.1007/s10853-011-5661-y
[21] T.J. Huang, X. Yin, G. Qi, Phys. Status. Solidi RRL, **8**, 735 (2014). https://doi.org/10.1002/pssr.201409219
[22] A. Ali, J. Jacob, M.I. Arshad, M.A. Nabi, A. Ashfaq, K. Mahmood, N. Amin, *et al*., Solid. State Sci. **103**, 106198 (2020). https://doi.org/10.1016/j.solidstatesciences
[23] U.V. Ghorpade, M.P. Suryawanshi, S.W. Shin, I. Kim, S.K. Ahn, J.H. Yun, and J.H. Kim, Chem. Mater. **28**, 3308 (2016). https://doi.org/10.1021/acs.chemmater.6b00176
[24] B. Saparov, Chem. Rev. **122**, 10575 (2022). https://doi.org/10.1021/acs.chemrev.2c00346
[25] U.A. Shah, A. Wang, M.I. Ullah, M. Ishaq, I.A. Shah, Y. Zeng, and K. Sun, Small, **20**, 2310584 (2024). https://doi.org/10.1002/smll.202310584
[26] Lalarukh, S.M. Hussain, S. Ali, A.F. Zahoor, H. Azmat, N. Nazish, M.A. Alshehri, *et al*., Polym. Adv. Technol. **35**, e6471 (2024). https://doi.org/10.1002/pat.6471
[27] H. Zhou, W.C. Hsu, H.S. Duan, B. Bob, W. Yang, T.B. Song, and Y. Yang, Energy Environ. Sci. **6**, 2822 (2013). https://doi.org/10.1039/C3EE41627E
[28] Y. Bellal, A. Bouhank, D. Belfennache, R. Yekhlef, East Eur. J. Phys. (1), 170 (2025). https://doi.org/10.26565/2312-4334-2025-1-16
[29] A. Urbina, J Phys Energy, **2**, 022001 (2020). https://doi.org/10.1088/2515-7655/ab5eee
[30] M.F. Islam, N.M. Yatim, P. Chelvanathan, M.T. Ferdaous, M.A. Hashim, A.K. Modak, N. Amin, Malaysian J. Sci. Health. Technol. **7**, 110 (2020). https://doi.org/10.33102/mjosht.v7io.117
[31] M. Wang, M. He, L. Zhu, B. Ma, F. Zhang, P. Liang, X. Chao, *et al*., J. Mater. Chem. A., **10**, 12946 (2022). https://doi.org/10.1039/D2TA02888C
[32] M.H. Sayed, M.M. Gomaa, and M. Boshta, Results. Opt. **12**, 100499 (2023). https://doi.org/10.1016/j.rio.2023.100499
[33] O.V. Parasyuk, L.D. Olekseyuk, and O.V. Marchuk, J. Alloys Compd. **287**, 197 (1999). https://doi.org/10.1016/S0925-8388(99)00047-X
[34] S.B. Jathar, S.R. Rondiya, Y.A. Jadhav, D.S. Nilegave, R.W. Cross, S.V. Barma, M.P. Nasane, *et al*., Chem. Mater. **33**, 1983 (2021). https://doi.org/10.1021/acs.chemmater.0c03223
[35] A.C. Lokhande, R.B.V. Chalapathy, M. He, E. Jo, M. Gang, S.A. Pawar, and J.H. Kim, Sol. Energy. Mater. Sol. Cells, **153**, 84 (2016). https://doi.org/10.1016/j.solmat.2016.04.003
[36] A.C. Lokhande, K.V. Gurav, E. Jo, C.D. Lokhande, and J.H. Kim, J. Alloys. Compd. **656**, 295 (2016). https://doi.org/10.1016/j.jallcom.2015.09.232
[37] A.C. Lokhande, K.V. Gurav, E. Jo, M. He, C.D. Lokhande, and J.H. Kim, Opt. Mater. **54**, 207 (2016). https://doi.org/10.1016/j.optmat.2016.02.040
[38] T.A. Kuku, and O.A. Fakolujo, Energy Mater. **16**, 199 (1987). https://doi.org/10.1016/0165-1633(87)90019-0
[39] J. Koike, K. Chino, N. Aihara, H. Araki, R. Nakamura, K. Jimbo, and H. Katagiri, Jpn. J. Appl. Phys., **51**, 10 (2012). https://doi.org/10.1143/JJAP.51.10NC34
[40] M. Umehara, Y. Takeda, T. Motohiro, T. Sakai, H. Awano, and R. Maekawa, J. Neurol. Sci. **146**, 167 (1997). https://doi.org/10.1016/S0022-510X(96)00301-2
[41] G.E. Delgado, A.J. Mora, G. Marcano, and C. Rincón, Mater. Res. Bull. **38**, 1949 (2003). https://doi.org/10.1016/j.materresbull.2003.09.017
[42] A.D. Dugarte, N.R. Pineda, L. Nieves, J.A. Henao, G.D. Delgado, and J.M. Delgado, Acta. Cryst. B, **77**, 158 (2021). https://doi.org/10.1107/S2052520620016571
[43] C. Wu, Z. Hu, C. Wang, H. Sheng, J. Yang, and Y. Xie, Appl. Phys. Lett. **91**, 143104 (2007). https://doi.org/10.1063/1.2790491
[44] D. Avellaneda, M.T.S. Nair, and P.K. Nair, J. Electrochem. Soc. **157**, D346 (2010). https://doi.org/10.1149/1.3384660
[45] M. Adelifard, M.M.B. Mohagheghi, and H. Eshghi, Phys. Scr. **85**, 035603 (2012). https://doi.org/10.1088/0031-8949/85/03/035603
[46] X. Chen, H. Wada, A. Sato, and M. Mieno, J. Solid. State. Chem. **139**, 144 (1998). https://doi.org/10.1006/jssc.1998.7822
[47] V. Roblés, J.F. Trigo, C. Guillén, and J. Herrero, J. Alloys. Compd. **642**, 40 (2015). https://doi.org/10.1016/j.jallcom.2015.04.104
[48] R. Bodeux, J. Leguay, and S. Delbos, Thin Solid Films, **582**, 229 (2015). https://doi.org/10.1016/j.tsf.2014.09.023
[49] J. Chang, and E.R. Waclawik, Cryst. Eng. Comm. **15**, 5612 (2013). https://doi.org/10.1039/C3CE40284C
[50] Y.T. Zhai, S. Chen, J.H. Yang, H.J. Xiang, X.G. Gong, A. Walsh, J. Kang, *et al*., Phys. Rev. B, **84**, 075213 (2011). https://doi.org/10.1103/PhysRevB.84.075213
[51] Y. Dong, J. He, X. Li, W. Zhou, Y. Chen, L. Sun, P. Yang, *et al*., Mater. Lett. **160**, 468 (2015). https://doi.org/10.1016/j.matlet.2015.08.028

[52] Q. Chen, X. Dou, Y. Ni, S. Cheng, and S. Zhuang, J. Colloid Interface Sci. **376**, 327 (2012). https://doi.org/10.1016/j.jcis.2012.03.015
[53] Y. Benkrima, D. Belfennache, R. Yekhlef, and A.M. Ghaleb, Chalcogenide Lett. **20**, 609-618 (2023). https://doi.org/10.15251/CL.2023.208.609
[54] K. Schwarz, P. Blaha, Comput. Mater. Sci. **28**, 259 (2003). https://doi.org/10.1016/S0927-0256(03)00112-5
[55] Y. Achour, Y. Benkrima, I. Lefkaier, and D. Belfennache, J. Nano- Electron. Phys. **15**(1), 01018(5pp) (2023). https://doi.org/10.21272/jnep.15(1).01018
[56] Y. Benkrima, D. Belfennache, R. Yekhlef, M.E. Soudani, A. Souiga, and Y. Achour, East Eur. J. Phys. (2), 150 (2023). https://doi.org/10.26565/2312-4334-2023-2-14
[57] Y. Benkrima, S. Benhamida, and D. Belfennache, Dig. J. Nanomater. Bios. **18**(1), 11 (2023) https://doi.org/10.15251/DJNB.2023.181.11
[58] Y. Benkrima, M.E. Soudani, D. Belfennache, H. Bouguettaia, and A. Souigat, J. Ovonic. Res. **18**(6), 797 (2022). https://doi.org/10.15251/JOR.2022.186.797
[59] A. Djemli, M. Reffas, K. Bouferrache, F. Benlakhdar, R. Yekhlef, D. Belfennache, S.I. Ahmed, *et al*., Phys. Solid State, **67**(5), 356 (2025). https://doi.org/10.1134/S1063783425600499
[60] K. Madoui, A Ghechi, S. Madoui, R. Yekhlef, D. Belfennache, S. Zaiou, and M.A. Ali, East Eur. J. Phys. (3), 390 (2024). https://doi.org/10.26565/2312-4334-2024-3-48
[61] E. Danladi, M. Kashif, A. Ichoja, and B.B. Ayiya, Trans. Tianjin. Univ. **29**, 62 (2023). https://doi.org/10.1007/s12209-022-00343-w
[62] A. Maoucha, T. Berghout, F. Djeffal, and H. Ferhati, Sol. Energy, **287**, 113251 (2025). https://doi.org/10.1016/j.solener.2025.113251
[63] I.D. Mayergoyz, J. Appl. Phys. **59**, 195 (1986). https://doi.org/10.1063/1.336862
[64] P. Lazzeretti, J. Chem. Phys. **151**, 114108 (2019). https://doi.org/10.1063/1.5124250
[65] A.N. Tuama, L.H. Alzubaidi, M.H. Jameel, K.H. Abass, M.Z.H. Mayzan, and Z.N. Salman, J. Sol-Gel. Sci. Technol. **110**, 792 (2024). https://doi.org/10.1007/s10971-024-06385-x
[66] F.D. Murnaghan, **30**, 244 (1944). https://doi.org/10.1073/pnas.30.9.244
[67] T. Raadik, M. Grossberg, J. Krustok, M. Kauk-Kuusik, A. Crovetto, R.B. Ettlinger, O. Hansen, *et al*., Appl. Phys. Lett. **110**, 261105 (2017). https://doi.org/ 10.1063/1.4990657
[68] T. Nomura, T. Maeda, T. Wada, Prog. Photovolt. Res. Appl. **20**, 520 (2012). https://doi.org/10.1002/pip.2183
[69] M. Onoda, X.A. Chen, A. Sato, and H. Wada, Mater. Res. Bull. **35**, 1563 (2000). https://doi.org/10.1016/S0025-5408 (00)00347-0
[70] M. Mesbahi, M.L. Benkhedir, UPB Sci. Bull. Ser. A, **79**, 293 (2017). https://doi.org/10.1103/PhysRevResearch.4.033067
[71] A. Kanai, K. Toyonaga, K. Chino, H. Katagiri, and H. Araki, Jpn. J. Appl. Phys. **54**, 08KC06 (2015). https://doi.org/10.7567/JJAP.54.08KC06
[72] J.D. De Wild, E.V.C. Robert, B.E. Adib, D. Abou-Ras, and P.J. Dale, Sol. Energy. Mater. Sol. Cells. **157**, 259 (2016). https://doi.org/10.1016/j.solmat.2016.04.039
[73] V.I. Anisimov, J. Zaanen, and O.K. Andersen, Phys. Rev. B, **44**, 943 (1991). https://doi.org/10.1103/PhysRevB.44.943
[74] A. Shigemi, T. Maeda, and T. Wada, Phys. Status Solidi B, **252**, 1230 (2015). https://doi.org/10.1002/pssb.201400346
[75] V.L. Shaposhnikov, A.V. Krivosheeva, V.E. Borisenko, and J.L. Lazzari, Sci. Jet. **1**, 1–4 (2012).
[76] T. Ouslimane, L. Et-taya, L. Elmaimouni, and A. Benami, Heliyon, **7**, e06379 (2021). https://doi.org/10.1016/j.heliyon.2021.e06379
[77] A.A. Kanoun, M.B. Kanoun, A.E. Merad, and S. Goumri-Said, Sol. Energy. **182**, 237 (2019). https://doi.org/10.1016/j.solener.2019.02.041
[78] M.K. Das, S. Panda, and N. Mohapatra, Mater. Today Proc. **74**, 756 (2023). https://doi.org/10.1016/j.matpr.2022.11.031
[79] S. Ahmed, F. Jannat, M.A.K. Khan, and M.A. Alim, Optik, **225**, 165765 (2021). https://doi.org/10.1016/j.ijleo.2020.165765
[80] A.N. Abena, A.T. Ngoupo, F.A. Abega, and J.M.B. Ndjaka, Chinese J. Phys. **76**, 94 (2022). https://doi.org/10.1016/j.cjph.2021.12.024
[81] M. Burgelman, P. Nollet, and S. Degrave, Thin Solid Films, **361–362**, 527 (2000). https://doi.org/10.1016/S0040-6090(99)00825-1
[82] F.E. Ikuemonisan, Y.O. Kayode, and O.B. Odubote, Next Materials, **8**, 100870 (2025). https://doi.org/10.1016/j.nxmate.2025.100870
[83] D. Belfennache, D. Madi, N. Brihi, M.S. Aida, and M.A. Saeed, Appl. Phys. A, **124**, 697 (2018). https://doi.org/10.1007/s00339-018-2118-z
[84] R. Ouldamer, D. Belfennache, D. Madi, R. Yekhlef, S. Zaiou, and M.A. Ali, J. Ovonic. Res. **20**(1), 45 (2024). https://doi.org/10.15251/JOR.2024.201.45
[85] D. Belfennache, D. Madi, R. Yekhlef, L. Toukal, N. Maouche, M.S. Akhtar, and S. Zahra, Semicond. Phys. Quant. Optoelectron. **24**(4), 378 (2021). https://doi.org/10.15407/spqeo24.04.378

## ДОСЛІДЖЕННЯ СТРУКТУРНИХ, ОПТОЕЛЕКТРОННИХ ТА ФОТОВОЛЬТАЇЧНИХ ХАРАКТЕРИСТИК СПОЛУКИ $Cu_2SnS_3$: КОМПЛЕКСНЕ DFT ТА SCAPS-1D МОДЕЛЮВАННЯ

**Буалем Када[1], Каріма Беньяхія[1], Набіл Белуфа[2,3], Хамза Рекаб-Джабрі[2,4], Д. Белфеннаше[5], Абделькадер Бухенна[1], Самір Бекхейра[2], А. Аламі[6], Хамад М. Адресс Хасан[7], Хамді А. Хатаб Алі[8]**

*[1]Лабораторія матеріалознавства та застосувань (LSMA), Факультет наук і технологій, Університет Айн-Темушент, Алжир*
*[2]Лабораторія мікро- та нанофізики (LaMiN), Національна політехнічна школа Оран, ENPO-MA, BP 1523, Ель-М'Науер, 31000, Оран, Алжир*
*[3]Гідрометеорологічний інститут навчання та досліджень IHFR, Ібну Рошд. Bp 7019, Оран, Алжир*
*[4]Факультет наук про природу та життя та наук про Землю, Університет АклІМоханд-Ульхадж, 10000, Буйра, Алжир*
*[5]Дослідницький центр промислових технологій (CRTI), поштова скринька 64, Черага 16014, Алжир, Алжир*
*[6]Лабораторія технологічних процесів, матеріалів та навколишнього середовища, Технологічний факультет, Університет Джиллалі Ліабес, поштова скринька А/с 89, Сіді-Бель-Аббес 22000, Алжир*
*[7]Кафедра хімії, факультет природничих наук, Університет Омара аль-Мухтара, Лівія*
*[8]Кафедра хімії, факультет освіти (Аль-Мардж), університет Бенгазі, Лівія*

Оцінка структурних, оптоелектронних та фотоелектричних характеристик сполуки $Cu_2SnS_3$ є важливою для розробки матеріалів для сонячної енергетики. Цей потрійний халькогенідний напівпровідник вирізняється сильним потенціалом у фотоелектричних застосуваннях завдяки широкому діапазону поглинання світла та хімічній стабільності. У цій статті ми дослідили структурні та оптоелектронні властивості потрійних напівпровідників на основі міді, зокрема тих, що входять до складу сполуки $Cu_2SnS_3$, а також їхню ефективність у фотоелектричних застосуваннях. Оскільки в попередніх дослідженнях існували значні відмінності щодо значень ширини забороненої зони (0,65-1,35 еВ), було зроблено спробу знайти відповідне наближення для вивчення цього типу сполуки. Структурні властивості досліджувалися з використанням як форми узагальненого градієнтного наближення (GGA) Пердью-Берка-Ернцергофа (PBE), так і наближення локальної густини (LDA), що дозволяє провести порівняльну оцінку впливу різних обмінно-кореляційних функціоналів на структуру матеріалу. Враховуючи важливий вплив, який деелектрони Cu відіграють на визначення їхніх електронних властивостей, як показано результатами, отриманими при використанні різних функціоналів обмінної кореляції енергії, для систематичної оптимізації розрахованого зміщення аніонів було використано комбіновану функцію потенціалу Бекке-Джонсона, модифікованого Траном та Блахою, та потенціалу Хаббарда (TB-mBJ+U). Розрахунки дали значення ширини забороненої зони. Енергія напівпровідникової квазічастинки в моноклінній структурі (m-CTS; SG: Cc) становить 0,7 еВ, а в орторомбічній структурі (золото-CTS; SG: Imm2) – 0,73 еВ, що значною мірою узгоджується з експериментальними значеннями. Дослідження оптичних властивостей, включаючи діелектричну функцію, також виявило коефіцієнт відбиття, коефіцієнт поглинання та показник заломлення сполуки $Cu_2SnS_3$ у двох її фазах. Останню вважають перспективним кандидатом для оптоелектронних застосувань. Для перевірки цього ми використали програму SCAPS, і результати були хорошими. Коли ця сполука використовується як абсорбуючий шар у фотоелектричному елементі, густина струму (Jsc) збільшується, досягаючи піку при товщині 800 нм.

**Ключові слова:** *$Cu_2SnS_3$; FP-LAPW; LDA; TB-mBJ+U; фотоелектричні елементи*